Available online at www.sciencedirect.com
SCIENCE DIRECT®
Journal of Molecular Catalysis A: Chemical 225 (2005) 149–160
JOURNAL OF MOLECULAR CATALYSIS A: CHEMICAL
www.elsevier.com/locate/molcata

C–X bond reactivity in the catalytic hydrodehalogenation of haloarenes over unsupported and silica supported Ni

K.V. Murthy[a], Patricia M. Patterson[b], Mark A. Keane[a,*]

[a] *Department of Chemical and Materials Engineering, University of Kentucky, Lexington, KY 40506, USA*
[b] *Center for Applied Energy Research, University of Kentucky, Lexington, KY 40506, USA*

Received 3 June 2004; received in revised form 31 August 2004; accepted 31 August 2004
Available online 8 October 2004

Abstract

The hydrodehalogenation (HDH) of fluorobenzene (FB), chlorobenzene (CB), bromobenzene (BB), iodobenzene (IB), 1,3-dichlorobenzene (1,3-DCB), 1,3-dibromobenzene (1,3-DBB) and 1,3-bromochlorobenzene (1,3-BCB) has been studied over Ni/SiO_2 at 573 K. In the case of the mono-haloarenes, HDH activity decreased in the order FB > CB > BB > IB, an effect that is discussed in terms of halogen inductive effects. The conversion of the di-substituted benzenes (at a common inlet X/Ni molar ratio) was significantly lower (by a factor of up to 2) than that recorded for the mono-haloarenes, i.e. the presence of a second electron withdrawing halogen substituent lowered the overall level of HDH. A decline in HDH activity with time-on-stream was observed in every instance. Catalyst activation via direct temperature-programmed reduction (TPR) has been monitored with on-line thermogravimetric/mass spectrometric/thermal conductivity analyses. The incorporation of a calcination step prior to reduction resulted in a marked decline in HDH activity. The pre- and post-reaction catalyst samples have been characterized by BET area measurements, X-ray diffractograms (XRD) and H_2 chemisorption/temperature-programmed desorption. TPR analyses of the post catalysis (passivated) samples were also conducted and compared with the response recorded for the unused catalysts. The loss of activity is linked to halogen/Ni interactions resulting in a suppression of H_2 uptake with possible Ni sintering and a disruption of the H_2/catalyst interactions. In the hydrotreatment of 1,3-BCB, the level of debromination exceeded that of dechlorination, a result that we attribute to a surface hydrochlorination and Cl exchange with the Br substituent on the aromatic ring. This effect extends to reactions over bulk NiO and $NiO + SiO_2$ mixtures.

Keywords: Hydrodehalogenation; Chlorobenzene(s); Bromobenzene(s); Fluorobenzene; Iodobenzene; Chlorobromobenzene; Nickel/silica

1. Introduction

Organohalogens are classified as high priority pollutants due to their toxicity, mutagenicity and carcinogenicity [1]. These compounds are of commercial significance in the manufacture of pesticides, plasticizers and disinfectants, processes that are potential sources of release into the environment [2] with associated ecological damage and atmospheric ozone depletion effects [3]. As a direct consequence, the safe handling/disposal of halogenated compounds is a pressing remediation issue. There are several technologies currently in use, i.e. incineration, pyrolysis, hydrolysis, chemical/biodegradation [4,5] but each can lead to the formation of other halogenated toxins and do not constitute the best practicable environmental option. Catalytic hydrodehalogenation (HDH) is now emerging as a viable alternative non-destructive treatment that can generate compounds of economic value from halogenated waste [6]; this report focuses on a Ni/SiO_2 promoted transformation of gaseous Cl-, Br-, I- and F- aromatics. The hydrodechlorination (HDC) of aliphatic organochlorines ($C_2H_3Cl_3$, C_2HCl_3, C_2Cl_4, CH_2Cl_2, $CHCl_3$ and CCl_4) has been investigated over Ni/SiO_2 (50 atm/573 K) [7,8] where significant catalyst deactivation was observed and attributed to coke formation via reactant polymerization. In the HDH (1 atm/523–563 K) of CH_2Cl_2 and $CHClF_2$ over bulk Ni and

* Corresponding author. Tel.: +1 859 257 5857; fax: +1 859 323 1929.
E-mail address: makeane@engr.uky.edu (M.A. Keane).

1381-1169/$ – see front matter © 2004 Elsevier B.V. All rights reserved.
doi:10.1016/j.molcata.2004.08.038

Ni/C, Ni carbide formation was proposed and found to be more active than the starting Ni phase [9]. The HDC of 1,2-$C_4H_8Cl_2$, an epichlorohydrin production by-product, has been examined over (5–40%, w/w) Ni/SiO_2 where a high selectivity (95%) to C_4H_8 was achieved and catalyst stability was attributed to the formation of Ni-hydrosilicate that was resistant to deactivation [10].

Focusing on haloarenes, HDC activity in the conversion of chlorobenzene (CB) over Ni/SiO_2 and Ni/C was found to be dependent on the nature of the support, activation conditions and Ni particle size, a response that is suggestive of HDC structure sensitivity [11,12]. The gas phase HDC of polychlorinated aromatics such as 1,2-dichlorobenzene (1,2-DCB), 1,2,4-trichlorobenzene (1,2,4-TCB) and hexachlorobenzene has been reported for Ni supported on Al_2O_3, $NiAl_2O_4$, hydrotalacites, MCM-41 and Cr_2O_3 where a high selectivity (>95%) to benzene has been linked to metal dispersion allied to the availability of surface reactive hydrogen [13–17]. Hydrodebromination (HDB), by comparison, has received less attention in the literature and few published articles of direct relevance could be found. The liquid phase HDB of hexabromobenzene and tribromobenzenes has been considered where a Pd metallocenyl diphosphine complex served as the (homogeneous) catalytic agent [18]. Yu et al. [19] recorded HDB activity for Pd anchored on polyvinyl pyrrolidone (PVP) and observed a decline in performance that was ascribed to HBr poisoning. Pd supported on $SiO_2/AlPO_4$, ZrO_2 and MgO was found to be active in the liquid phase HDH of 1,3-bromochlorobenzene (1,3-BCB) [20,21]. We have shown elsewhere [22,23] that gas phase HDH of a range of substituted bromo- and chloroarenes over supported Ni is 100% selective in terms of C–X bond scission with no aromatic ring reduction, where electron donating ring substituents serve to raise the overall reaction rate. Marques et al. [24] have studied the liquid phase HDB of dibromobenzene(s) (DBB) over Pd/C and Raney-Ni catalysts in mixed organic/aqueous media and found the Pd/C to be significantly more active. An exhaustive search through the literature failed to unearth any studies of gas phase HDH of iodobenzene (IB) or fluorobenzene (FB) over supported Ni. It is, however, worth flagging studies of liquid phase hydrodeiodination (with molecular hydrogen) of IB over Pd/C [25,26] and the liquid phase hydrodefluorination of FB and 1,2-difluorobenzene where Rh complexes tethered to a silica support [27,28] and Zr-based organometallics (homogeneous system) [29] served as the catalytic agents.

In this investigation, we report reproducible activities/selectivities for the gas phase HDH of FB, CB, BB, IB, 1,3-DCB, 1,3-DBB and 1,3-BCB over unsupported and SiO_2 supported Ni and focus on the relative reactivity of the C–Cl, C–Br, C–I and C–F bonds for hydrogen scission. We have carefully monitored catalyst activation (reduction with/without precalcination) and have examined the changes to the catalyst structure that result during HDH.

2. Experimental

2.1. Catalyst preparation and activation

A 10% (w/w) (determined by ICP-OES, Vista-PRO, Varian Inc.) Ni on SiO_2 (fumed, Aldrich) precursor was prepared by standard impregnation, where an aqueous nickel nitrate solution was added drop wise to the substrate at 343 K with constant agitation; the catalyst precursor was washed with deionized water and dried in air at 383 K. Prior to use in catalysis, the precursor, sieved (ATM fine test sieves) into a batch of 75 μm average particle diameter, was reduced directly in a 60 $cm^3\,min^{-1}$ stream of ultra pure H_2 at 10 K min^{-1} to 723 ± 1 K, which was maintained for 12 h. Alternatively, the catalyst precursor was subjected to a precalcination step, i.e. heating in air at 10 K min^{-1} to 873 K (maintained for 1 h), cooling in He to room temperature with a subsequent reduction in H_2 (as above) but to a final temperature of 873 K. Unsupported NiO, and a physical mixture (thorough mixing was ensured) of $NiO + SiO_2$ and $Ni(NO_3)_2 + SiO_2$ were also employed where the Ni content in the mixture = 10% (w/w) Ni.

2.2. Catalyst characterization

After reduction (as above) or after catalysis, the sample was flushed for 1 h in a stream of He, cooled (in He) to room temperature and passivated in (40 $cm^3\,min^{-1}$) 1% (v/v) O_2/He; there was no detectable temperature increase during sample passivation. This treatment served to provide a protective oxide layer over the surface Ni that prevented bulk oxidation upon exposure to the atmosphere. The BET surface area, temperature-programmed reduction (TPR), H_2 chemisorption and temperature-programmed desorption (TPD) associated with the freshly activated (pre- and post-passivation) and spent (passivated) samples were determined using the commercial CHEM-BET 3000 (Quantachrome) unit. The samples were loaded into a U-shaped Pyrex glass cell (10 cm × 3.76 mm i.d.) and heated in 20 $cm^3\,min^{-1}$ (mass flow controlled) 5% (v/v) H_2/N_2 to 723 K at 10 K min^{-1}. The effluent gas passed through a liquid N_2 trap and H_2 consumption was monitored by a thermal conductivity detector (TCD) with data acquisition/manipulation using the TPR Win™ software. The samples were maintained at 723 K for 12 h in a steady flow of H_2; TPR was also monitored following the precalcination outlined above (with an ultimate reduction temperature = 873 K). The reduced samples were swept with a 20 $cm^3\,min^{-1}$ flow of N_2 for 1 h at the final reduction temperature, cooled to room temperature and subjected to H_2 chemisorption using a pulse (50–100 μl) titration procedure: detectable uptake >0.2 cm^3 H_2 at STP per gram Ni. The samples were thoroughly flushed with pure N_2 (20 $cm^3\,min^{-1}$) for 30 min to remove physisorbed H_2. Temperature-programmed desorption was conducted in the N_2 flow at 50 K min^{-1} to 723 K. BET areas were recorded with a 30% (v/v) N_2/He flow; pure N_2 (99.9%) served as the internal stan-

dard. At least two cycles of nitrogen adsorption–desorption in the flow mode were employed to determine total surface area using the standard single point method. BET surface area and hydrogen uptake values were reproducible to within ±5% and the values quoted in this paper are the mean. BJH pore volume analyses were performed using the commercial Micromeritics TriStar 3000 unit; the catalyst precursor and activated (with and without precalcination) samples exhibited a cumulative pore volume = $2.2 \pm 0.2\ cm^3\ g^{-1}$ with an average pore radius = 22 ± 2 nm. Temperature-programmed treatment was also undertaken using a Seiko Instruments Inc. TG/DTA 320 simultaneous thermo-gravimetric/differential thermal analyser coupled to a micromass PC residual gas analyser. A known quantity of catalyst (ca. 18 mg) was placed in a Pt sample pan and subjected to the same temperature ramping sequence(s), in either a reducing (20%, v/v, H_2/He) or an oxidizing (30%, v/v, air/He) flow, while monitoring the effluent gas over the mass range 10–100. Powder X-ray diffractograms (XRD) were recorded with a Philips X'Pert instrument using Ni-filtered Cu Kα radiation. The samples were mounted in a low background sample holder and scanned at a rate of $0.02^\circ\ step^{-1}$ over the $30 \leq 2\theta \leq 90^\circ$ range with a scan time of $5\ s\ step^{-1}$. The diffractograms were compared with the JCPDS-ICDD [30] references for identification purposes.

2.3. Catalysis procedure

Reactions were carried out under atmospheric pressure, in situ immediately after activation, in a fixed bed glass reactor (i.d. = 15 mm) at 573 K. The catalytic reactor, and operating conditions to ensure negligible heat/mass transport limitations, have been described in detail elsewhere [31] but some features, pertinent to this study, are given below. All the chemicals (FB, CB, BB, IB, 1,3-DCB, 1,3-DBB and 1,3-BCB supplied by Aldrich with >99.8% purity) were fed (undiluted or in methanol) by means of a microprocessor controlled infusion pump (Model 100, kd Scientific) via a glass/teflon air tight syringe and a teflon line to the reactor in a stream of ultra pure H_2 (GHSV = $1200\ h^{-1}$), the flow rate of which was monitored using a Humonics 520 digital flow meter. The reactant inlet molar flow rate was in the overall range 9×10^{-3} to $2 \times 10^{-2}\ mol\ h^{-1}$ where H_2 was maintained in at least 20 times excess relative to stoichiometric quantities; all the reactants were used without further purification. In a series of blank tests, passage of each reactant in a stream of H_2 through the empty reactor, i.e. in the absence of catalyst, did not result in any detectable conversion. Moreover, reaction of the haloarenes over silica alone was not accompanied by any detectable HDH: the presence of Ni (supported or unsupported) is essential for H_2 scission activity. The reaction products were collected over a period of 24 h (6–8 h in the case of the physical mixtures) and analyzed by capillary GC as described elsewhere [32]. Catalytic HDH is quantified in this report on the basis of fractional dehalogenation (α_X) and

$$\alpha_X = \frac{[HX]_{out}}{[X]_{in}} (X = F, Cl, Br, I) \quad (1)$$

benzene selectivity ($S_{benzene}$), taking the conversion of 1,3-DCB

$$S_{benzene} = \frac{[benzene]_{out}}{[1,3\text{-DCB}]_{in} - [1,3\text{-DCB}]_{out}} \times 100 \quad (2)$$

where [X] represents the aromatic halogen concentration, [HX] the concentration of hydrogen halide product and in/out refers to the inlet/outlet streams. A halogen (in the form of HX) mass balance was performed by passing the effluent gas through an aqueous NaOH trap ($3.5–8.0 \times 10^{-3}\ mol\ dm^{-3}$, kept under constant agitation at 400 rpm) with independent pH (Hanna HI Programmable Printing pH Bench-Meter) and potentiometric (Metrohm Model 728 Autotitrys) analyses. Repeated (up to five separate) catalytic runs with different samples from the same batch of catalyst delivered product compositions that were reproducible to within ±7%.

3. Results and discussion

3.1. Catalyst characterization: pre-reaction

The BET surface area of the freshly activated (unused) catalyst is recorded in Table 1 along with the H_2 chemisorption values. Hydrogen uptake on the Ni/SiO_2 precursor reduced in situ was essentially the same as that recorded after TPR of the passivated/reduced sample, indicative of an equivalency of both activation routes. The controlled room

Table 1
BET surface areas and H_2 chemisorption values associated with the unused and spent catalysts

Sample	BET surface area ($m^2\ g^{-1}$)	H_2 chemisorption ($cm^3\ g_{Ni}^{-1}$)
Activated[a] Ni/SiO_2, unused	190	10.4
Activated[b] Ni/SiO_2, unused	195	10.7
Precalcined/activated Ni/SiO_2[b], unused	185	1.5
Ni/SiO_2 after FB HDF[a]	183	6.1
Ni/SiO_2 after CB HDC[a]	180	4.6
Precalcined and activated Ni/SiO_2 after CB HDC[a]	173	0.8
Ni/SiO_2 after 1,3-DCB HDC[a]	175	2.7
Ni/SiO_2 after BB HDB[a]	189	2.5
Ni/SiO_2 after 1,3-DBB HDC[a]	184	1.3
Ni/SiO_2 after 1,3-BCB HDH[a]	185	1.7
Ni/SiO_2 after IB HDI[a]	178	2.3
Activated NiO[b], unused	6	–[c]
Activated NiO + SiO_2 physical mix[b], unused	185	–[c]
Activated $Ni(NO_3)_2$ + SiO_2 physical mix[b], unused	190	–[c]

[a] Analysis of a passivated sample.
[b] In situ analysis.
[c] Below detection limits.

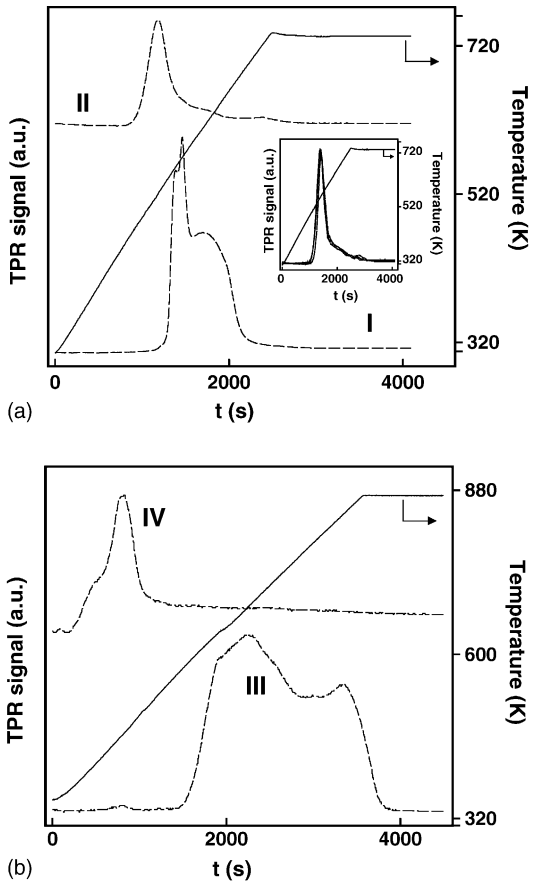

Fig. 1. (a) TPR profiles generated for direct reduction of the Ni/SiO_2 precursor to 723 K pre-passivation (I) and post-passivation (II) (inset shows the results of repeated TPR runs) passivation. (b) TPR profiles generated for reduction to 873 K of the precalcined (at 873 K) Ni/SiO_2 precursor pre-passivation (III) and post-passivation (IV).

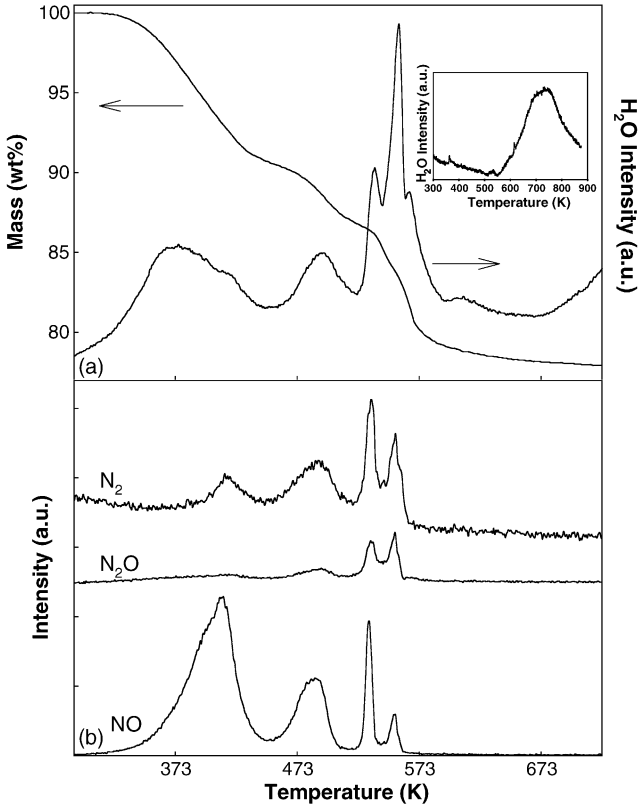

Fig. 2. (a) Mass (wt.%), water signal intensity and (b) nitrogen, nitrous oxide and nitric oxide signal intensity as a function of temperature in the direct reduction of the Ni/SiO_2 precursor to 723 K. Inset to (a) H_2O profile generated during the heat treatment of the SiO_2 support in flowing H_2 under the same conditions used in the direct reduction of Ni/SiO_2.

temperature passivation provided a protective oxide coating over the supported metal, permitting storage/transfer for directly meaningful ex situ analyses. The TPR profiles generated for the direct reduction of the Ni/SiO_2 precursor without (to 723 K, profile I) and with (profile III) precalcination (to 873 K) and those associated with a "re-reduction" of the same samples after passivation (profiles II and IV) are given in Fig. 1. The degree of TPR reproducibility is illustrated in the inset to Fig. 1a which shows three separate TPR profiles, taking the post-passivated direct TPR sample (profile II) as a representative case. The direct reduction of the Ni/SiO_2 generated a sharp H_2 consumption peak at 560 K with an ill-defined lower temperature (548 K) shoulder and a secondary broader higher temperature H_2 consumption with an associated $T_{max} = 615$ K. The lower temperature peak(s) has(have) been attributed [33,34] to the decomposition of nickel nitrate to NiO. A subsequent reduction of NiO to Ni^0 is responsible for the higher T_{max} peak—Mizushima et al. [35] in their TPR study of a 10% (w/w) impregnated Ni/SiO_2 have attributed a TPR T_{max} at ca. 630 K to NiO reduction. Montes et al. [36] likewise ascribed a TPR maximum at 651 K to reduction of NiO on a 15% (w/w) impregnated Ni/SiO_2 while Gonzlez-Marcos and co-workers [37] linked their single TPR peak at 601 K for impregnated Ni/SiO_2 directly to $Ni(NO_3)_2$ decomposition. We have extended our TPR analysis by monitoring the decomposition (in H_2) of the nitrate precursor by thermogravimetic analysis where the effluent gas was analyzed using on-line mass spectrometry: the results are included in Fig. 2, wherein a weight loss in excess of 20% is in evidence. Jackson et al. [38] have reported a similar TPR weight loss profile, but without on-line MS analysis, for the activation of 1% (w/w) Ni/SiO_2. Our MS results demonstrate that precursor decomposition generated peaks at m/e of 18, 28, 30 and 44 amu which we assigned to H_2O, N_2, NO and N_2O respectively; NO_2 (main fragment at $m/e = 30$) release cannot be discounted. $N_2/NO/H_2O$ predominate at $T < 523$ K with concomitant $N_2/N_2O/NO/H_2O$ release at $T > 523$ K. The occurrence of a H_2O release maximum at 566 K (Fig. 2a) without an accompanying $N_2/N_2O/NO$ (Fig. 2b) evolution suggests a reduction of NiO to Ni^0 that precedes the higher temperature reduction demonstrated by profile I in Fig. 1a. This is also validated by the differential thermal analysis, (not shown), where the presence of a sharp exotherm was associated with the peak at 566 K. A generation of zerovalent Ni at yet lower temperatures is possible but an explicit distinction between precursor decomposition and metal formation is not possible

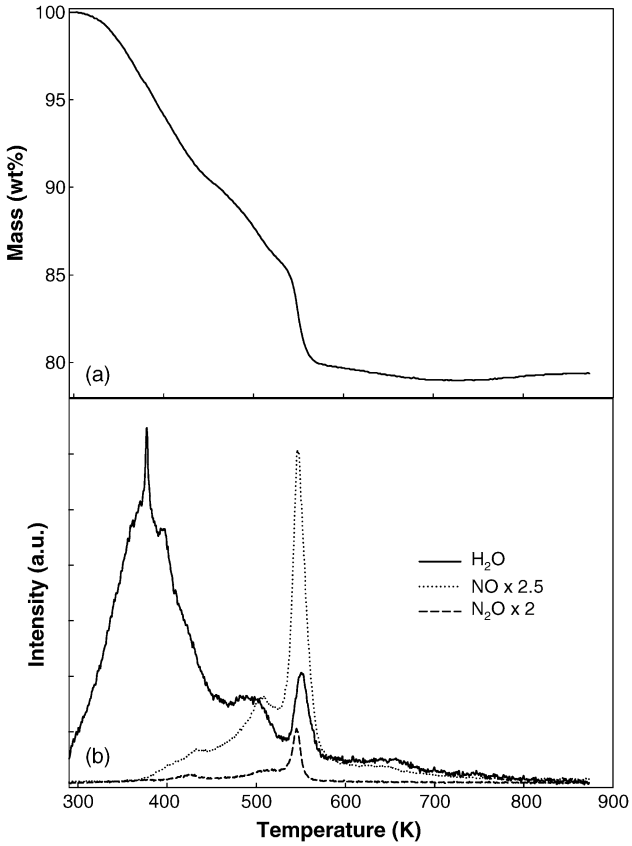

Fig. 3. (a) Mass (wt.%) and (b) water, nitric oxide and nitrous oxide signal intensity as a function of temperature during the calcination of the Ni/SiO_2 precursor in air to 873 K.

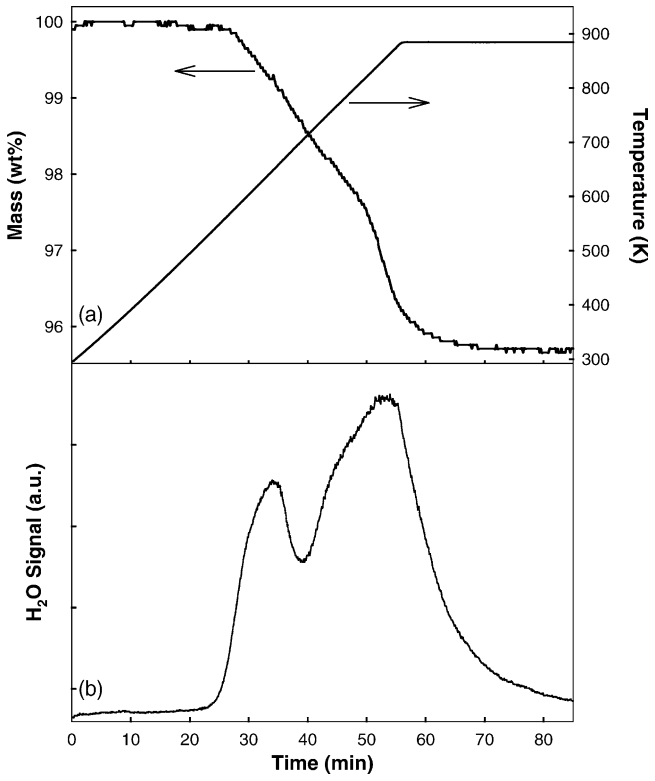

Fig. 4. (a) Mass (wt.%) and (b) water signal intensity resulting from the reduction (to 873 K) of the precalcined (see Fig. 3 Ni/SiO_2).

at $T < 560$ K where the profiles represent composite temperature effects. The decomposition/reduction of a supported metal salt is a complex multi-step solid-phase reaction where heterogeneity in nucleation site density/oxide particle size will result in a range of temperature dependent reductions. It is worth flagging the apparent emergence of a H_2O peak at the completion of the direct Ni/SiO_2 reduction: see Fig. 2a. In a separate run, we recorded the H_2O profile generated during the heat treatment of the SiO_2 support in flowing H_2 under the same conditions used in the direct reduction of Ni/SiO_2. The resultant profile is recorded as an inset to Fig. 2a where a H_2O release at T_{max} = ca. 740 K can be observed which matches the emerging peak in Fig. 2a. This water loss can be attributed to a thermally induced dehydroxylation of the SiO_2 support, as has been noted elsewhere [39–41].

The introduction of a calcination step prior to reduction had a significant effect on the subsequent TPR profile (III, see Fig. 1b), which was characterized by a broad T range (from ca. 600 to >800 K) of H_2 consumption with an ill-defined T_{max} at ca. 740 K. Geus et al. [42] have also recorded a broad reduction peak (T_{max} at 743 and 773 K) during the TPR of Ni/SiO_2 precalcined at 573 K. Our precalcination step alone resulted in a 20% weight loss (Fig. 3a) with water, nitric oxide and nitrous oxide the significant components in the effluent (Fig. 3b), where the principal release of the nitrogen oxides occurred at a similar temperature (540–550 K) to that observed during precursor decomposition in H_2 (Fig. 2b). Mile et al. [34] observed weight loss maxima at 537 and 559 K in the thermal decomposition of silica supported nickel nitrate and inferred, without any mass spectroscopic gas analysis of the effluent gas, an associated decomposition of $Ni(NO_3)(OH)\ 2.5H_2O$ to NiO with release of HNO_3 and H_2O. The mass of the calcined sample was 2.24% greater (from TGA) than that after H_2 treatment, which agrees well with the expected mass difference between the NiO and Ni^0 content in the respective samples. Thermogravimetric/mass spectrometric analysis of the reduction step that followed precalcination revealed a slight weight loss (<5%, see Fig. 4a) and water release (Fig. 4b), produced by the reduction of NiO, over the temperature range corresponding to that observed for H_2 consumption (see Fig. 1b, profile III). It is evident, from a comparison of profiles I and III in Fig. 1, that the incorporation of a precalcination step has rendered the supported nickel phase more difficult to reduce, a response that finds agreement in the literature where an increase in the precalcination temperature is accompanied by a higher TPR T_{max} [34,43]. The incorporation of a calcination step has been proposed to generate nickel hydrosilicate that is more difficult to reduce [33,38,44]. Both passivated samples are characterized by a single reduction peak (Fig. 1) that arose at a lower temperature for the precalcined (ca. 450 K) when compared with the uncalcined sample (ca. 510 K): a TGA/MS analysis of the

TPR of the passivated samples revealed only the presence of water in the effluent gas. As is to be expected, the reduction of these passivated samples is far more facile than the activation of the starting catalyst precursors. Vos et al. [45] have studied the TPR of (37 and 56%, w/w) Ni/Al_2O_3 samples after passivation and recorded one peak at 473 K, which they assigned to the reduction of the passivating oxide layer. Hadjiivanov et al. [46] likewise noted a significant shift in the reduction peak for 1.7% (w/w) Ni/SiO_2 (prepared by a grafting technique) to 489 K after passivation. It is known from the literature [33,47,48] that a precalcination of an impregnated Ni/SiO_2 precursor results in an appreciable increase in Ni particle size after reduction and this is borne out by the substantial reduction in H_2 uptake (Table 1); the requirement of a higher reduction temperature for the calcined sample should also contribute to metal sintering. The lower TPR T_{max} value associated with the passivated precalcined sample is then diagnostic of a more facile reduction of the poorly dispersed metal phase.

An interpretation of these TPR profiles is further facilitated by comparison with those generated (under identical conditions) for bulk NiO and physical mixtures of $NiO + SiO_2$ and $Ni(NO_3)_2 + SiO_2$, which are included in Fig. 5. The single H_2 consumption peak associated with the direct reduction of bulk NiO and the physical mix with SiO_2 can be linked to the higher T_{max} recorded for the direct reduction of Ni/SiO_2. The discernible shift (to higher T) in the reduction peak for the mixture may be attributed to some interaction of NiO with SiO_2 as has been observed by Ermakova and Ermakov [49]. A subsequent passivation resulted in a bulk oxide phase that was readily reduced in a subsequent TPR as is evident from a consideration of profiles (c) and (e) in Fig. 5. It should be noted that the chemical interaction that is prevalent in the passivated Ni/SiO_2 (profile (a), Fig. 5) necessitates a higher treatment temperature for the removal of the passivation layer. The direct reduction of $Ni(NO_3)_2 + SiO_2$ generated a broad region of H_2 consumption where $T > 540$ K (profile (f), Fig. 5) that can be attributed to a combined concomitant $Ni(NO_3)_2$ decomposition/NiO reduction (see Fig. 2); subsequent passivation and TPR again generated a low temperature indistinct peak. Following TPR, there was no detectable hydrogen uptake on the starting bulk NiO or the $NiO + SiO_2$ and $Ni(NO_3)_2 + SiO_2$ mixture; any H_2 chemisorption was below detection limits.

The XRD patterns for the passivated unused Ni/SiO_2 samples, with/without precalcination are given in Fig. 6, where the similarity of each is evident. The three peaks at 44.5°, 51.8° and 76.3°, corresponding to (1 1 1), (2 0 0) and (2 2 0) planes of metallic nickel present in each sample are consistent with an exclusive cubic symmetry; the markers included in Fig. 6 illustrate the position and relative intensity of the XRD peaks for cubic Ni taken from the JCPDS standards [30]. Taking the signal at 44.5°, the peak width at half height, i.e. the standard peak broadening approximation, suggests a larger Ni particle size associated with the precalcined sample, in accordance with the H_2 chemisorption data. It is instructive to note that there was no evidence of bulk NiO, i.e. the reduction procedure was fully effective in reducing the metal component to zero valent Ni while the passivation step served to provide a protective oxide coating on the metal with no bulk NiO formation. Hydrogen temperature-programmed desorption (H_2 TPD) can shed some light on the electronic properties of supported metal particles [50]; the H_2 TPD profiles for the unused and spent (to be discussed later) samples are presented in Fig. 7. A diversity of H_2 desorption patterns have been reported in the literature

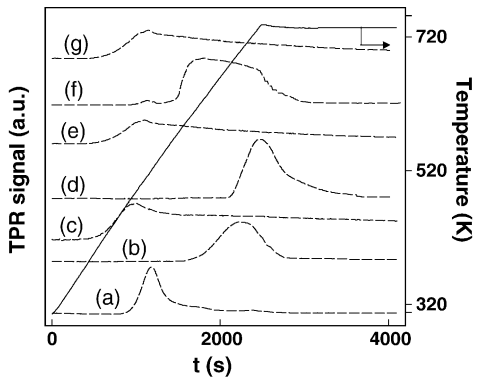

Fig. 5. TPR profiles generated for: (a) passivated Ni/SiO_2 (without precalcination), bulk NiO; (b) pre-passivation; (c) post-passivation, $NiO + SiO_2$ (10%, w/w, Ni) physical mix; (d) pre-passivation; (e) post-passivation and $Ni(NO_3)_2 + SiO_2$ (10 %, w/w, Ni); (f) pre-passivation; and (g) post-passivation.

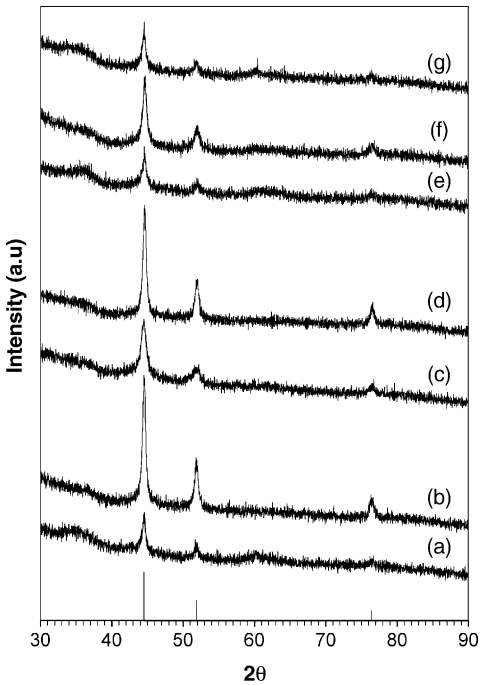

Fig. 6. XRD patterns for the passivated unused activated Ni/SiO_2 without (a) and with (b) precalcination, the spent uncalcined (c) and precalcined (d) sample after CB HDC and the spent uncalcined sample after (e) FB HDF, (f) BB HDB and (g) IB HDI. Note: the solid lines indicate peak position (with relative intensity) for cubic Ni.

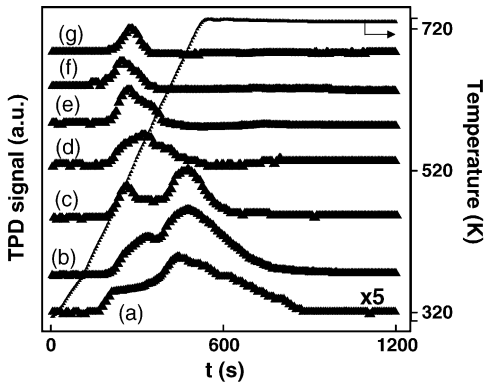

Fig. 7. H_2-TPD profiles associated with passivated Ni/SiO_2: (a) calcined/reduced at 873 K and the passivated sample reduced directly at 723 K without precalcination; (b) unused; (c) after CB HDC; (d) after BB HDB; (e) after 1,3-DCB HDC; (f) after 1,3-DBB HDB; (g) after 1,3-BCB HDH.

with both low (<600 K) and high (>600 K) temperature peaks where any associated T_{max} is strongly influenced by the desorption conditions/experimental procedures [51–55]. The H_2 TPD profiles generated for activated unused Ni/SiO_2 with/without precalcination are characterized by a principal desorption peak (660–690 K) with a secondary lower temperature release (500–560 K). Given the lower H_2 uptake associated with the precalcined sample, the TPD profile has been magnified to aid comparison—it can be seen that the combined precalcination/higher reduction temperature step had little effect on the overall H_2 release characteristics, albeit the (ill-defined) T_{max} was shifted to a lower value.

3.2. Hydrodehalogenation activity/selectivity

Hydrodehalogenation of FB, CB, BB, IB, 1,3-DCB, 1,3-DBB and 1,3-BCB over Ni/SiO_2 at 573 K generated benzene and, in the case of the di-substituted arenes, CB and BB as the only products: secondary hydrogenation to yield cyclohexene/cyclohexane or bromo-/chlorocyclohexane/cyclohexene was not observed. The latter suggests that the dehalogenated products once generated desorb from the catalyst without any ring reduction, as noted previously [56] for HDH over supported Ni. In contrast, a secondary ring reduction has been reported elsewhere [57,58] for HDC over Pd, Rh and Pt-based catalysts. Fractional HDH (α_X), over the directly reduced Ni/SiO_2, under identical reaction conditions is illustrated as a function of time-on-stream for the four mono-halogenated arene reactants in Fig. 8. In each case, there was a drop in the level of dehalogenation before the ultimate attainment of a steady state conversion; the precalcined/reduced Ni/SiO_2 showed the same decline in α_X with time-on-stream. The temporal response of α_X can be expressed in terms of the empirical relationship

$$\frac{\alpha_X - \alpha_0}{\alpha_{ss} - \alpha_0} = \frac{\Delta t}{\beta + \Delta t} \quad (3)$$

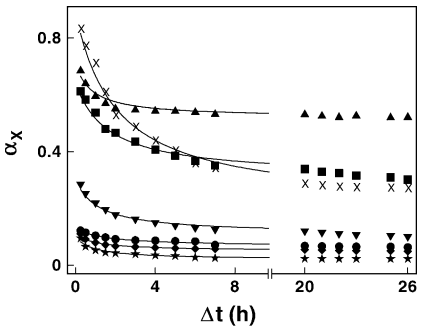

Fig. 8. Fractional dehalogenation (α_X) as a function of time-on-stream for the conversion of FB (×), CB (▲), BB (●), IB (⋆), 1,3-DCB (■) 1,3-DBB (♦) and 1,3-BCB (▼): $W/F = 10\ g\ mol_X^{-1}\ h$. Note: lines represent fits to Eq. (3).

where α_{ss} represents the steady state fractional conversion and β is a time scale fitting parameter. Fit convergence yields values for α_0, the initial fractional HDH and $\Delta t_{0.8}$, the time required for the fractional dehalogenation to decay to 80% of its initial value, two indices on which to base a comparison of haloarene reactivity: these values are recorded in Table 2. Taking the α_0 values as a measure of initial activity under fixed bed plug-flow operation where H_2 was maintained far in excess, the following reactor/kinetic expression applies

$$\ln(1 - \alpha_0)^{-1} = k\left(\frac{W}{F_X}\right) \quad (4)$$

where F_X is the inlet molar halogen feed rate ($mol_X\ h^{-1}$) and W the catalyst mass; the parameter W/F_X (units, $g\ h\ mol_X^{-1}$) has the physical significance of contact time. From a consideration of gas phase reaction equilibrium constants [59], the dehalogenation step(s) under the stated reaction conditions can be taken to be irreversible. The linear relationships between $\ln(1 - \alpha_0)^{-1}$ and W/F_X for each mono-haloarene are shown in Fig. 9; each line passes through the origin, diagnostic of adherence to pseudo-first order kinetics. The extracted pseudo-first order rate constants support the following sequence of increasing reactivity: IB ($k = 11 \times 10^{-3}$ $mol\ h^{-1}\ g^{-1}$) < BB ($k = 15 \times 10^{-3}\ mol\ h^{-1}\ g^{-1}$) < CB ($k = 12 \times 10^{-2}\ mol\ h^{-1}\ g^{-1}$) < FB ($k = 22 \times 10^{-2}\ mol\ h^{-1}\ g^{-1}$). On the basis of C–X bond dissociation energy, the ease of reductive dehalogenation should follow the reverse order, i.e. C–I (53 kcal mol^{-1}) > C–Br (67 kcal mol^{-1}) > C–Cl

Table 2
Initial fractional dehalogenation (α_0) and the time required for the fractional dehalogenation to decay to 80% of this initial value ($\Delta t_{0.8}$): $W/F = 10$ ($g\ mol_X^{-1}\ h$)

Reactant	α_0	$\Delta t_{0.8}$ (h)
FB	0.89	1.3
CB	0.71	3.1
BB	0.13	1.0
IB	0.10	0.3
1,3-DCB	0.64	1.1
1,3-DBB	0.11	0.7
1,3-BCB	0.30	0.8

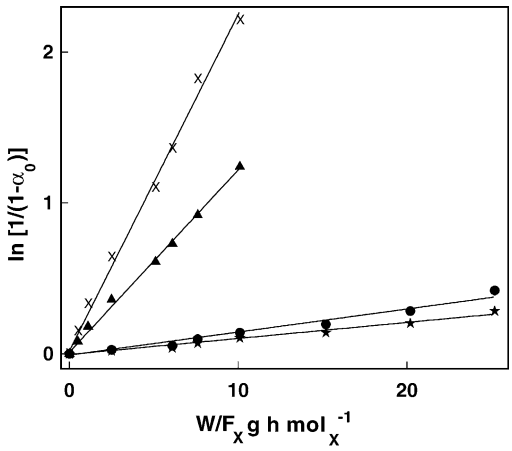

Fig. 9. Pseudo-first order relationships for the hydrodehalogenation of FB (×), CB (▲), BB (●), and IB (⋆).

(81 kcal mol^{-1}) > C–F (109 kcal mol^{-1}) [60,61]. Indeed, this reactivity sequence was found to hold in the liquid phase dehalogenation of alkyl halides using both a homogeneous Ni catalyst [62] and Raney Ni [63], a trend that has been found to extend to the catalytic transfer hydrodehalogenation of aliphatic halides (in 2-propanal/NaOH) over Pd/C [64] and the dehalogenation of haloarenes by Pd/C in a mixed (isooctane/KOH/quaternary onium salt) solution phase [24,25]. However, in gas phase heterogeneously catalyzed HDH, the general consensus of opinion that is now emerging from the literature [6,65–67] supports a surface mechanism involving dissociative adsorption of the haloarene with the formation of a surface σ-complex via the aromatic ring carbon with the highest electron density. As the inductive effect associated with halogen substituents increases from I to F, the electron density of the ring (C–X) carbon in IB is lower than that associated with FB with a consequent decrease in haloarene reactivity [68], as observed in this study. The reactivity of both DCB and DBB, on the basis of the tabulated α_0 values, is significantly lower than that associated with the corresponding mono-haloarene while the degree of dehalogenation of the BCB reactant falls within these two extremes. Catalyst deactivation was more appreciable (see lower $\Delta t_{0.8}$ values in Table 2) during the processing of the disubstituted haloarenes. The presence of the second electron withdrawing Cl and Br in 1,3-DCB, 1,3-DBB and 1,3-BCB has an overall deactivating effect with the result that the entire halogen complement is less susceptible to hydrogen cleavage. A precalcination of the Ni/SiO_2, which impacted on TPR/H_2 uptake behavior (see Figs. 1–3/Table 1), served to significantly lower the initial HDH activity (by a factor of three), as revealed in Table 3. Nevertheless, the latter was still greater than that generated by bulk NiO. The mixed NiO + SiO_2 (and $Ni(NO_3)_2$ + SiO_2) systems delivered slightly higher dehalogenation activities than NiO alone, a response that can be linked to the inferred (from the TPR response in Fig. 5) metal/silica interaction and/or involvement of spillover hydrogen [14,69,70] where Ni acts as a dissociation center for hydrogen that then spills

Table 3
Initial fractional dehalogenation (α_0) of CB and BB over Ni/SiO_2 (with/without precalcination), bulk NiO, and NiO + SiO_2 and $Ni(NO_3)_2$ + SiO_2 physical mixtures: W/F = 10 (g mol$_X^{-1}$ h)

Catalyst	α_0	
	CB feed	BB feed
Ni/SiO_2 reduced at 723 K	0.71	0.13
Ni/SiO_2 precalcined/reduced at 873 K	0.23	0.04
NiO reduced at 723 K	0.04	<0.01
NiO + SiO_2 reduced at 723 K	0.06	0.01
$Ni(NO_3)_2$ + SiO_2 reduced at 723 K	0.06	0.01

over to the silica. Indeed, we have shown elsewhere [67] that CB HDC kinetics can be accounted for on the basis of reaction between non-competitively and dissociatively adsorbed chloroaromatic and spillover hydrogen.

The relationship between benzene selectivity ($S_{benzene}$) and the fractional conversion of the three di-halosubstituted aromatics is shown in Fig. 10a. The greater reactivity of the Cl substituents in DCB for hydrogen scission is immediately apparent where both the fractional conversion of 1,3-DCB ($\alpha_{1,3\text{-DCB}}$) and associated benzene selectivity ($S_{benzene}$) are so much higher that there is no possible overlap with either the 1,3-DBB and 1,3-BCB profiles, which are essentially equivalent. The HDH of the di-haloarenes can proceed in a parallel/series stepwise fashion where the mono-halorene serves as a reactive intermediate [59]. The greater degree of dechlo-

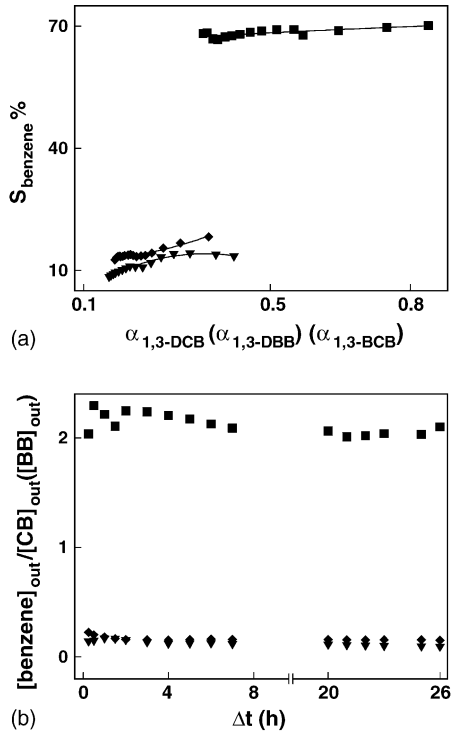

Fig. 10. (a) Benzene selectivity ($S_{benzene}$) as a function of the fractional conversion (α) of 1,3-DCB (■) 1,3-DBB (♦) and 1,3-BCB (▼). (b) Ratio of benzene (complete dehalogenation) to halo-benzene (CB or BB, i.e. partial dehalogenation) in the reactor effluent, symbols as above: inlet molar W/F = 10 g mol$_X^{-1}$ h.

Table 4
Outlet (out) to inlet (in) aromatic Br concentration ratio, at selected reaction times for the conversion of BB and 1,3-BCB; $W/F = 10$ (g mol$_{Br}^{-1}$ h)

Δt (h)	$[Br]_{out}/[Br]_{in}$	
	BB feed	1,3-BCB feed
0.25	0.79	0.58
1	0.84	0.63
4	0.87	0.78
8	0.90	0.82
24	0.91	0.85

rination is further established in Fig. 10b where the temporal response of total relative to partial HDH is plotted—total dehalogenation is preferred in the case of 1,3-DCB whereas a partial HDH predominates in the conversion of 1,3-DBB and 1,3-BCB. One unexpected selectivity response was the absence of any BB component in the effluent from the 1,3-BCB feed—the catalyst was 100% selective in terms of HDB and CB was the only partially dehalogenated intermediate. Given the appreciably higher reactivity of CB/DCB compared with BB/DBB, it was expected that the organobromine content in the effluent gas from BCB hydroprocessing should far exceed that of organochlorine. Rather, the presence of the Cl substituent on the benzene ring served to promote HDB as can be seen from the entries in Table 4 where Br removal (relative to the inlet feed) is compared under identical reaction conditions (same $[Br]_{in}$) for the conversion of BB and 1,3-BCB. A similar observation was recorded elsewhere for the HDH of a mixed CB + BB feed over supported Ni and was ascribed to a halogen exchange reaction [23]. This effect was further probed by considering the HDH of 1,3-BCB over bulk NiO and the NiO + SiO_2 physical mix: the results are presented in Fig. 11. The fractional dehalogenation over bulk NiO was raised slightly with the addition of SiO_2 (Fig. 11a), as observed earlier (Table 3) for the conversion of CB and BB. Indeed, the incorporation of SiO_2 in the Ni/SiO_2 bed also served to raise α_X when compared with the undiluted Ni/SiO_2 (see Fig. 11a). Spillover hydrogen can again be invoked to account for the promotional effect of SiO_2; a temporal loss of activity was observed for each system. The ratio of aromatic Br/Cl in the effluent stream fell below 1 for the conversion of 1,3-BCB over the four catalyst systems. This is in marked contrast to that expected on the basis of CB HDC and BB HDB, as illustrated in Fig. 11b where the "predicted" ratio far exceeds unity. There was no evidence of BB in the product stream associated with reaction over NiO (with/without SiO_2 addition). Any HDC must serve to chlorinate the surface, as shown elsewhere [71], with a subsequent exchange reaction where the adsorbed aromatic carbonium ion intermediate is attacked by surface HCl; HBr must not participate in an analogous bromination step to the same extent. Indeed, Br displacement from aromatic nuclei has been found to be more facile than that of Cl in catalyzed vapor phase halogen exchange reactions [72,73]. The enhanced degree of debromination is then the result of a combined HDB and hydrochlorination (Cl exchange) as composite steps in the removal of Br from the aromatic host. The degree of debromination, in terms of the aromatic $[Br]_{out}/[Br]_{in}$ ratio was directly proportional to the fractional 1,3-BCB conversion ($\alpha_{1,3\text{-BCB}}$) where reaction over supported and unsupported Ni with/without SiO_2 addition delivered a common trend line, shown in Fig. 11c.

3.3. Catalyst characterization: post-reaction

BET surface area analysis (Table 1) before and after catalysis demonstrated that there was no appreciable change in overall area. Moreover, chemical analysis (ICP-OES) of the activated catalysts pre- and post-reaction did not reveal any measurable loss of Ni as a result of catalysis. However, the TPR characteristics of the spent samples, used to promote an array of HDH reactions, deviated significantly from the profile associated with the unused sample: the passivated used samples exhibited a principal TPR peak that arose at temperatures up to 60 K lower when compared with the passivated unused catalyst, as illustrated in Fig. 12. In addition, the level of H_2 chemisorbed on the spent samples, as recorded in Table 1, was considerably lower. The latter response is indicative of Ni particle growth during reaction and Ni sintering as a result of HDC has been noted previously [10,23,74,75] and can be ascribed to a halide-induced agglomeration of Ni particles [76] due to the surface mobility of Ni–X species [77]. In a recent study [78], we clearly demonstrated (from TEM analysis) growth of Ni particles during hydrodehalogenation over Ni/SiO_2. The shift in the TPR maximum peak to lower temperatures is in line with a more facile reduction of the (HDH induced) sintered metal phase. The XRD profiles associated with representative spent samples are included in Fig. 6. There was no observable bulk NiO or Ni halide phase in the catalysts after use but, as XRD is a bulk structural characterization tool, we do not discount the possible formation of surface halide species. Indeed, we have shown elsewhere [23,74] that supported metal catalysts bear an appreciable surface HCl component during chloroarene HDC, some of which is irreversibly held and resistant to thermal desorption. Our XRD analysis confirm that an exclusive cubic Ni symmetry was maintained as opposed to the findings of Choi and Lee [10] which suggested a Ni (on SiO_2) phase transformation from cubic to hexagonal during 1,2-dichloropropane HDC. Moreover, there was no evidence of nickel carbide formation as has been reported by Morato et al. [9] during the hydro-conversion of CFC-12 and HFC-22 over Ni on carbonaceous supports. We subjected the passivated spent samples to a high temperature (298–1273 K) heat treatment in flowing H_2 with on-line mass spectroscopic analysis and recorded small weight changes (<2%). The latter was predominantly due to the loss of water associated with removal of the passivating oxide layer. There was no evidence of any significant methane generation—the latter should result from a hydrogasification of a structural Ni_3C phase but can be discounted in this instance. All the spent samples exhibited a shift in H_2 TPD to lower temperatures (see Fig. 7) and, with the exception of the sample used in CB

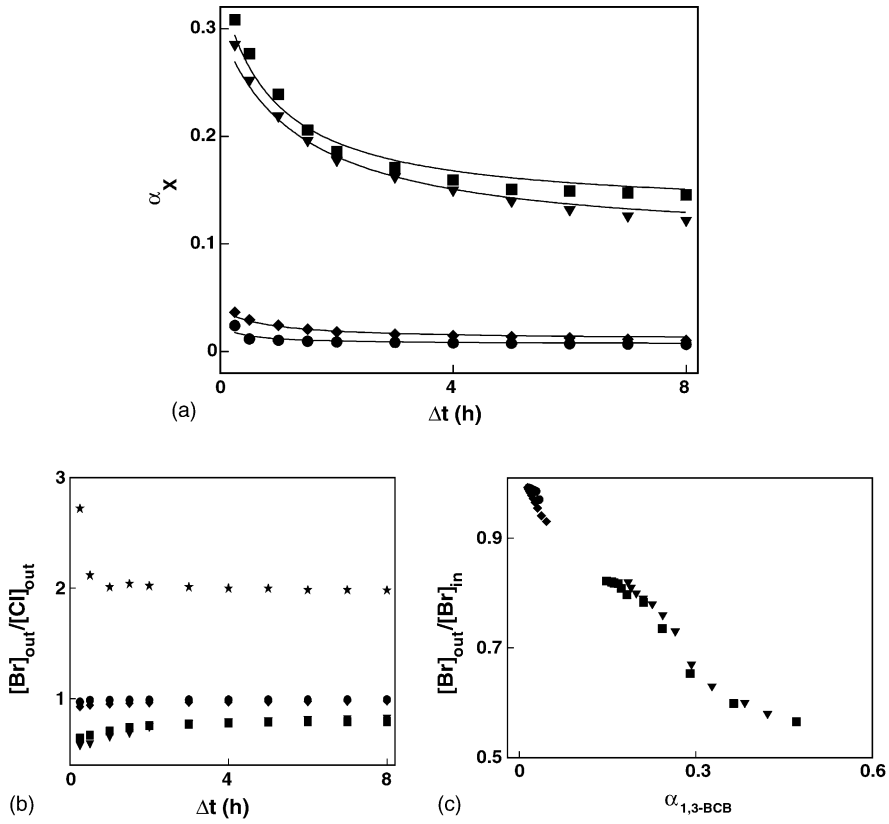

Fig. 11. (a) Fractional dehalogenation (α_X) as a function of time-on-stream for the conversion of 1,3-BCB over Ni/SiO_2 (▼), $Ni/SiO_2 + SiO_2$ (■), NiO (●) and $NiO + SiO_2$ (♦); lines represent fits to Eq. (3). (b) Ratio of aromatic Br to Cl in the outlet stream ($[Br]_{out}/[Cl]_{out}$) as a function of time-on-stream, symbols as above where (⋆) represents the predicted values based on CB HDC and BB HDB data. (c) Ratio of outlet to inlet aromatic Br concentration, ($[Br]_{out}/[Br]_{in}$) as a function of fractional 1,3-BCB conversion ($x_{1,3\text{-BCB}}$), symbols as above; $W/F = 10\ g\ mol_X^{-1}\ h$.

HDC, desorption was characterized by a single broad TPD peak with T_{max} in the range 500–560 K. It is known that halogens can act as electron acceptors with respect to supported transition metal systems [57,79] and the presence of Cl impacts on H_2 adsorption/desorption dynamics on Ni [51,52]. In this study, the shift in H_2 TPD T_{max} to lower values is diagnostic of weaker H/Ni interactions that results from extended catalyst HDH use. The characteristics of the spent catalysts that can be linked to the observed activity loss are reduced H_2 uptake that exhibits a weaker interaction with the catalyst.

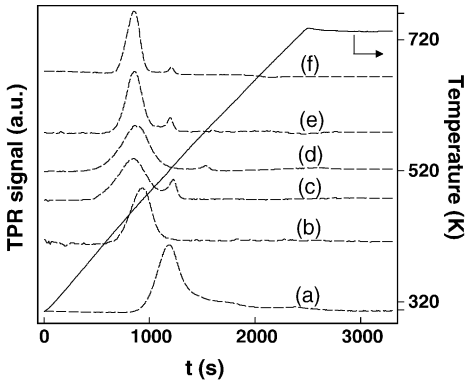

Fig. 12. TPR profiles generated for passivated Ni/SiO_2 reduced at 723 K without precalcination: (a) unused; (b) after CB HDC; (c) after BB HDB; (d) after 1,3-DCB HDC; (e) after 1,3-DBB HDB; and (f) after 1,3-BCB HDH.

4. Conclusions

HDH of FB, CB, BB, IB, DCB, DBB and BCB over Ni/SiO_2 yields the partially dehalogenated mono-haloarene (in the case of the di-substituted arenes) and benzene with no ring reduction. Mono-haloarene reactivity decreases (from FB to IB) with a decreasing halogen inductive contribution that serves to activate the C–X bond for hydrogenolytic attack. The presence of a second halogen ring substituent has a deactivating effect that lowers the overall HDH. However, the degree of debromination exceeded dechlorination in the case of the BCB reactant as a result of the reactivity of surface HCl which facilitates a hydrochlorination or Cl exchange with aromatic Br. Bulk NiO exhibited HDH activity that was raised with the addition of SiO_2 and the same trend of higher HDC relative to HDB for the conversion of mono (chloro- or bromo-) aromatics with an apparent Cl/Br exchange in the conversion of BCB. Activation of Ni/SiO_2 in H_2 involved a decomposition of the supported nitrate precursor (to generate N_2, N_2O, NO and H_2O and concomitant Ni^0) with a subse-

quent reduction of NiO to Ni^0. A precalcination of Ni/SiO_2 resulted in an appreciable alteration to the TPR characteristics, necessitating a higher reduction temperature leading to Ni sintering and an ultimate lower HDH activity. HDH over supported and unsupported Ni was subject to a temporal loss of activity that was accompanied by a disruption to the H_2 adsorption/desorption surface dynamics.

Acknowledgements

The authors are grateful to Antonio de Lucas Consuegra for his contribution to this work, which was supported in part by the National Science Foundation through Grant CTS-0218591.

References

[1] H.R. Bauser, Chemosphere 7 (1979) 415.
[2] D.G. Crosby, Environmental Toxicology and Chemistry, Oxford University Press, New York, 1998.
[3] L.E. Manzer, Catal. Today 13 (1992) 13.
[4] C. Seignez, A. Vuillenium, N. Adler, P. Peringer, J. Hazard. Mater. 84 (2001) 265.
[5] J. Frimmel, M. Zdrazil, J. Chem. Technol. Biotechnol. 63 (1995) 17.
[6] B.F. Hagh, D.T. Allen, Chem. Eng. Sci. 45 (1990) 2695.
[7] K.A. Frankel, B.W.L. Jang, G.W. Roberts, J.J. Spivey, Appl. Catal. A: Gen. 209 (2001) 401.
[8] S. Ordonez, H. Sastre, F.V. Diez, Appl. Catal. B: Environ. 25 (2000) 49.
[9] A. Morato, C. Alonso, F. Medina, P. Salagre, J.E. Sueiras, R. Terrado, A. Giralt, Appl. Catal. B: Environ. 23 (1999) 175.
[10] Y.H. Choi, W.Y. Lee, Catal. Lett. 67 (2000) 155.
[11] M.A. Keane, C. Park, C. Menini, Catal. Lett. 88 (2003) 89.
[12] N. Lingaiah, M.A. Uddin, A. Muto, T. Iwamoto, Y. Sakata, Y. Kusano, J. Mol. Catal. A: Chem. 161 (2000) 157.
[13] Y. Cesteros, P. Salagre, F. Medina, J.E. Sueiras, D. Tichit, B. Coq, Appl. Catal. B: Environ. 32 (2001) 25.
[14] Y. Cesteros, P. Salagre, F. Medina, J.E. Sueiras, Appl. Catal. B: Environ. 25 (2000) 213.
[15] Y. Cesteros, P. Salagre, F. Medina, J.E. Sueiras, Appl. Catal. B: Environ. 22 (1999) 135.
[16] Y. Cesteros, P. Salagre, F. Medina, J.E. Sueiras, Catal. Lett. 79 (2002) 83.
[17] Y.A. Serguchev, Y.V. Belokopytov, Kinet. Catal. 42 (2001) 174.
[18] B. Wei, S. Li, H.K. Lee, T.S.A. Hor, J. Mol. Catal. A: Chem. 126 (1997) 183.
[19] Z. Yu, S. Liao, Y. Xu, React. Funct. Polym. 29 (1996) 151.
[20] M.A. Aramendia, V. Borau, I.M. Garcia, C. Jimenez, J.M. Marinas, J. Urbano, Appl. Catal. B: Environ. 20 (1999) 101.
[21] M.A. Aramendia, V. Borau, I.M. Garcia, C. Jimenez, A. Marinas, J.M. Marinas, J. Urbano, Appl. Catal. B: Environ. 43 (2003) 71.
[22] C. Menini, C. Park, E.-J. Shin, G. Tavoularis, M.A. Keane, Catal. Today 62 (2000) 355.
[23] C. Park, C. Menini, J.L. Valverde, M.A. Keane, J. Catal. 211 (2002) 451.
[24] C.A. Marques, O. Rogozhnikova, M. Selva, P. Tundo, J. Mol. Catal. A: Chem. 96 (1995) 301.
[25] C.A. Marques, M. Selva, P. Tundo, J. Org. Chem. 58 (1993) 5256.
[26] Y. Ambroise, C. Mioskowski, G. Djega-Mariadassou, B. Rousseau, J. Org. Chem. 65 (2000) 7183.
[27] S.D. Brown, T.G. Richmond, Chemtracts 13 (2000) 134.
[28] H. Yang, H. Gao, R.J. Angelici, Organometalics 18 (1999) 2285.
[29] B.M. Kraft, R.J. Lachicotte, W.D. Jones, J. Am. Chem. Soc. 123 (2001) 10973.
[30] JCPDS—ICDD, PCPDFWIN, Version 2.2, June 2001.
[31] M.A. Keane, P.M. Patterson, J. Chem. Soc., Faraday Trans. 92 (1996) 1413.
[32] G. Yuan, M.A. Keane, Chem. Eng. Sci. 58 (2003) 257.
[33] C. Louis, Z.X. Cheng, M. Che, J. Phys. Chem. 97 (1993) 5703.
[34] B. Mile, D. Stirling, M.A. Zammitt, M.A. Lovell, M. Webb, J. Catal. 114 (1988) 217.
[35] T. Mizushima, K. Nishida, H. Ohkita, N. Kakuta, Bull. Chem. Soc. Jpn. 75 (2002) 2283.
[36] A. Diaz, D.R. Acosta, J.A. Odriozala, M. Montes, J. Phys. Chem. B 101 (1997) 1782.
[37] M.P. González-Marcos, J.I. Gutiérrez-Ortiz, C. González-Ortiz de Elguea, J.R. González-Velasco, J. Mol. Catal. A: Chem. 120 (1997) 185.
[38] S.D. Jackson, J. Willis, G.J. Kelly, G.D. McLellan, G. Webb, S. Mather, R.B. Moyes, S. Simpson, P.B. Wells, R. Whyman, Phys. Chem. Chem. Phys. 1 (1999) 2573.
[39] V.I. Bogillo, L.S. Pirnach, A. Dabrowski, Langmuir 13 (1997) 928.
[40] M.-A. Einasrud, L. Rørmark, S. Haereid, T. Grande, J. Non-Cryst. Solids 211 (1997) 49.
[41] J.H. Zimnoch dos Santos, C. Krug, M. Barbosa da Rosa, F.C. Stedile, J. Dupont, M. de Camargo Forte, J. Mol. Catal. A: Chem. 139 (1999) 199.
[42] J. van de Loosdrecht, A.M. van der Kraan, A.J. van Dillen, J.W. Geus, J. Catal. 170 (1997) 217.
[43] K. Hadjivanov, M. Mihaylov, D. Klissurski, P. Stefanov, N. Abadjieva, E. Vassileva, L. Mintchev, J. Catal. 185 (1999) 314.
[44] M.A. Keane, Can. J. Chem. 72 (1994) 372.
[45] B. Vos, E. Poels, A. Bliek, J. Catal. 198 (2001) 77.
[46] K. Hadjiivanov, M. Mihaylov, D. Klissurski, P. Stefanov, N. Abadjieva, E. Vassileva, L. Mintchev, J. Catal. 185 (1999) 314.
[47] M. Montes, C. Pennemann de Bosscheyde, B.K. Hodnett, F. Delannay, P. Grange, B. Delmon, Appl. Catal. 12 (1984) 309.
[48] G.A. Martin, C. Mirodatos, H. Praliaud, Appl. Catal. 1 (1981) 367.
[49] M.A. Ermakova, Y.D. Ermakov, Appl. Catal. A: Gen. 245 (2003) 277.
[50] E.-J. Shin, A. Spiller, G. Tavoularis, M.A. Keane, Phys. Chem. Chem. Phys. 1 (1999) 3173.
[51] J. Estelle, J. Ruz, Y. Cesteros, R. Fernandez, P. Salagre, F. Medina, J.-E. Sueiras, J. Chem. Soc., Faraday Trans. 92 (1996) 2811.
[52] S. Smeds, T. Salmi, L.P. Lindfors, O. Krause, Appl. Catal. A: Gen. 144 (1996) 177.
[53] J.A. Konvalinka, P.H. van Oeffelt, J.J.F. Scholten, Appl. Catal. 1 (1981) 141.
[54] G.D. Weatherbee, C.H. Bartholomew, J. Catal. 87 (1984) 55.
[55] A.G. Boudjahem, S. Monteverdi, M. Mercy, M.M. Bettahar, J. Catal. 221 (2004) 325.
[56] G. Tavoularis, M.A. Keane, J. Mol. Catal. 142 (1999) 187.
[57] B. Coq, G. Ferrat, F. Figueras, J. Catal. 101 (1986) 434.
[58] P. Bodnariuk, B. Coq, G. Figueras, J. Catal. 116 (1989) 459.
[59] E.J. Shin, M.A. Keane, Chem. Eng. Sci. 54 (1999) 1109.
[60] F. Alonso, I.P. Beletskaya, M. Yus, Chem. Rev. 102 (2002) 4009.
[61] I. Imamoto, in: B.M. Trost, M.I. Fleming (Eds.), Comprehensive Organic Synthesis, Pergamon Press, Oxford, 1991, p. 794.
[62] G.K. Lahiri, L.J. Schussel, A.M. Stolzenberg, Inorg. Chem. 31 (1992) 4991.
[63] A.F. Barrero, E.J. Alvarez-Manzaneda, R. Chahboun, R. Meneses, J.L. Romera, Synletters (2001) 485.
[64] Y. Usiku, T. Miyadera, Nippon Kagaku Kaishi (1998) 369; Y. Usiku, T. Miyadera, Chem. Abs. 128 (1998) 308213.
[65] Y.A. Serguchev, Y.V. Belokopytov, Kinet. Catal. 42 (2001) 174.
[66] M.A. Keane, D.Y. Murzin, in: D.G. Morrell (Ed.), Catalysis of Organic Reactions, Marcel Dekker, New York, 2002, p. 595.
[67] M.A. Keane, D.Y. Murzin, Chem. Eng. Sci. 56 (2001) 3185.

[68] J.W. Bozzelli, Y.M. Chen, S.S.C. Chuang, Chem. Eng. Commun. 115 (1992) 1.
[69] W.C. Conner Jr., G.M. Pajonck, S.J. Teichner, Adv. Catal. 34 (1986) 1.
[70] F. Benseradj, F. Sadi, M. Chater, Appl. Catal. A: Gen. 228 (2002) 135.
[71] G. Tavoularis, M.A. Keane, J. Chem. Technol. Biotechnol. 74 (1999) 60.
[72] S. Imhaoulene, L. Vivier, M. Guisnet, G. Perot, Tetrahedron 50 (1994) 12913.
[73] J. Lindley, Tetrahedron 40 (1984) 1433.
[74] M.A. Keane, in: M.A. Keane (Ed.), Interfacial Applications in Environmental Engineering, Marcel Dekker, New York, 2002, p. 231.
[75] A. Gampine, D. Eyeman, J. Catal. 179 (1998) 315.
[76] Y. Ohtsuka, J. Mol. Catal. 54 (1989) 225.
[77] C. Hoang-Van, Y. Kachaya, S.J. Teichner, J. Phys. Chem. B 101 (1997) 7060.
[78] K.V. Murthy, P.M. Patterson, G. Jacobs, B.H. Davis, M.A. Keane, J. Catal. 223 (2004) 74.
[79] T. Halchev, E. Ruckenstein, J. Catal. 73 (1982) 171.